Double ionization in *R*-matrix theory using a two-electron outer region

Jack Wragg, J. S. Parker, and H. W. van der Hart
Centre for Theoretical Atomic, Molecular and Optical Physics, School of Mathematics and Physics, Queen's University Belfast, Belfast BT7 1NN, United Kingdom
(Received 2 April 2015; published 10 August 2015)

We have developed a two-electron outer region for use within R-matrix theory to describe double ionization processes. The capability of this method is demonstrated for single-photon double ionization of He in the photon energy region between 80 and 180 eV. The cross sections are in agreement with established data. The extended R-matrix with time dependence method also provides information on higher-order processes, as demonstrated by the identification of signatures for sequential double ionization processes involving an intermediate He^+ state with $n = 2$.

DOI: 10.1103/PhysRevA.92.022504 PACS number(s): 31.15.A−, 32.80.Fb

I. INTRODUCTION

The development of laser sources capable of generating ultrashort light pulses or intense xuv and x-ray laser light [1–3] has put additional emphasis on the investigation of multiple ionization processes [4]. To complement recent experimental developments, there is a need for new computational techniques able to describe the multiple ionization of general atoms. Although progress has been made in the description of double photoionization of general atoms [5], further progress is needed to enable investigation of these processes in a time-dependent manner. This is of particular importance in experiments involving ultrashort light pulses.

One possible route to develop capability for the description of double-ionization processes is R-matrix theory. Time-independent R-matrix theory has already been extended for this purpose. The R-matrix with pseudostates technique (RMPS) utilizes a large basis set in the inner region, which includes residual-ion states in the continuum. Although the first electron can escape, the second must remain bound. Nevertheless, information on double ionization can be obtained through evaluating the probability that the residual ion is left in an excited state above the ionization threshold [6]. A second R-matrix approach for double ionization is the intermediate-energy R-matrix (IERM) theory, in which two electrons are allowed to escape the inner region. This leads to a two-dimensional propagation of the R matrix over a large distance where the R matrix is matched to asymptotic solutions. This approach was initially applied to scattering [7,8] and has recently been applied to double photoionization [9].

One promising computational method for solving the time-dependent Schrödinger equation (TDSE) for many-electron atoms in laser fields is R matrix with time dependence (RMT) [10–12]. With electron-electron interactions fully incorporated, RMT has been used to successfully model a number of features of many-electron atoms undergoing photoionization [13,14]. In RMT, an R-matrix basis set inner region [15] is attached to an outer-region finite difference grid [16] with the ability to describe an ionized electron, enabling the physical processes in each region to be modeled with an appropriate numerical method.

While previous applications of RMT to double ionization [17] have calculated accurate two-photon cross sections, the range of observables obtainable with this method is narrowed by an upper limit on the radial distance traveled by the inner ionizing electron, causing reflections upon interaction with the inner-region boundary. In this article, we report a method capable of modeling both ejected electrons accurately over a broad range of energies and integration volumes.

In the present approach, we adopt the philosophy of IERM theory within RMT theory by allowing two electrons to escape into the outer region. Electron i in the outer region is here described through a finite-difference (FD) representation for the radial coordinate r_i. We thus employ three distinct regions: (i) an inner region, in which all N electrons are within a distance a from the nucleus, represented with a standard R-matrix basis set, (ii) a one-electron outer region, in which we combine a basis-set representation for the residual system with $(N-1)$ electrons and an FD representation for the ionized electron with $r_N > a$, and (iii) a two-electron outer region, in which we use a basis-set representation for the residual system with $(N-2)$ electrons and an FD representation for the two electrons with $r_{N-1}, r_N > a$.

As a proof-of-principle, we apply it in the present article to single-photon double photoionization of He. This process has already been studied extensively, both experimentally [18] and theoretically [19,20], and it is therefore possible to compare the outcomes of the calculations with benchmark data. However, since the approach described here allows the simultaneous calculation of higher-order processes (such as double electron above threshold ionization [21]), we also expect signatures of these higher-order processes to appear in the results.

II. THEORETICAL AND COMPUTATIONAL APPROACH

The Hamiltonian for the helium atom in a laser field is given in atomic units (a.u.) as

$$\hat{H} = -\frac{1}{2}\nabla_1^2 - \frac{1}{2}\nabla_2^2 - \frac{2}{r_1} - \frac{2}{r_2} + \frac{1}{r_{12}} + E(t)(z_1 + z_2), \quad (1)$$

and the time-dependent Schrödinger equation is given by

$$i\frac{\partial \Psi}{\partial t} = \hat{H}\Psi. \quad (2)$$

In these equations, r_1 and r_2 are the radial coordinates of the first and second electrons, and $\frac{1}{r_{12}}$ represents the interelectron repulsion. $E(t)$ is the time-dependent laser field, and Ψ is the

two-electron wave function. z_1 and z_2 are the positions of the electron in the direction of the laser field.

The two-electron outer-region wave function is described on a set of two-dimensional FD grids given as $\Psi_q(r_1,r_2)$ where each grid describes the component of the wave function corresponding to the angular momentum quantum numbers $q = (\ell_1,\ell_2,L)$ across the coordinates $r_1 = a \ldots b$ and $r_2 = a \ldots b$. Near the boundary with the one-electron outer region ($r_1 \approx a$ and $r_2 \approx a$), the two-electron outer region is provided with the necessary wave function information from the one-electron outer region on an extension of the FD grid. This allows the direct evaluation of Eq. (2) using FD techniques.

In the one-electron outer region, the inner electron is described using a near-complete basis of eigenfunctions of He^+ within a box with free-boundary conditions: eigenfunctions of

$$\hat{H}_+ = -\frac{1}{2}\nabla_1^2 - \frac{2}{r_1} + L_b, \tag{3}$$

where L_b is a Bloch operator [15]. The outer electron is described using an FD representation. The presence of a Bloch operator for the inner electron leads to boundary derivative terms arising at the boundary between the one- and two-electron outer regions. As a consequence, the TDSE for the one electron outer region becomes

$$i\frac{\partial}{\partial t} f_p(r_2,t) = \hat{H} f_p(r_2,t) + \frac{1}{2}\sum_q \mathcal{A}\Omega_{pq} \frac{\partial \Psi_q(r_1,r_2)}{\partial r_1}\bigg|_{r_1=a}, \tag{4}$$

where $f_p(r_2,t)$ is an FD representation of the wave function at radial distance r_2 and time t in channel p. Ω_{pq} is the surface amplitude that links channel p to the two-electron FD grid $\Psi_q(r_1,r_2)$, and $\mathcal{A}$ is the antisymmetrization operator. This equation is similar to the propagation equation for inner-region single ionization RMT theory [11,12]. However, the final term on the right-hand side connects the wave function $f_p(r_2,t)$ in the one-electron outer region with the wave function $\Psi_q(r_1,r_2)$ in the two-electron outer region.

In the inner region, the propagation equations are identical to those in RMT theory for single ionization [11,12]:

$$\frac{d}{dt}C_k(t) = -i\sum_{k'} H_{kk'}C_{k'}(t) - \frac{i}{2}\sum_p \omega_{pk}\frac{\partial f_p(r_2,t)}{\partial r}\bigg|_{r=a}. \tag{5}$$

In this equation, the coefficients $C_k(t)$ are coefficients of the two-electron R-matrix basis functions in the inner region, and ω_{pk} are boundary amplitudes of the two-electron functions at the boundary $r_2 = a$.

RMT theory for single ionization has previously adopted Arnoldi propagators for time propagation, requiring separate propagators for the homogeneous TDSE and for each boundary term that contributed to the propagation. The complexity arising from multiple propagators is avoided here through the use of a simpler Taylor series computational scheme.

At each stage of the calculation, we consider the antisymmetry of the wave function under particle exchange. We have implemented this antisymmetry by considering the two-electron outer-region wave function for all $r_1 > a$ and $r_2 > a$. The link between the one-electron outer region and the two-electron outer region is taken along both boundaries of the two-electron outer region, $r_1 = a$, $r_2 \geqslant a$ and $r_1 \geqslant a$, $r_2 = a$. A phase change can be included to account for the spin symmetry of the electron pair.

Analysis of the final wave function occurs through projection of the final state onto uncorrelated products of eigenfunctions of the one-electron He^+ Hamiltonian: $F_{\ell_1}(E_1,r_1)F_{\ell_2}(E_2,r_2)$. As the two electrons travel far from the core and from each other, the energies can be interpreted as momenta $\mathbf{p}$ squared: $E_i = \mathbf{p_i}\cdot\mathbf{p_i}/2m = k_i^2\hbar^2/2m$, or in a.u., $k_i = \sqrt{2E_i}$. In this article we use k rather than E and generally refer to it as the momentum of the electron.

This approach is correct in the limit in which the two ejected electrons are sufficiently weakly interacting. In the present calculations we propagate the electrons for (typically) 70 field periods after the laser pulse has ramped to zero, during which time their Coulomb repulsion enhances their spatial separation. We note that k is derived from energy and includes contributions from the Coulomb potential, but these contributions appear to be negligible. If we allow the two-electron wave packet to depart the core for durations longer than the usual 70 field periods, then the calculated energy spectra do not change.

To separate the single-photon yield from the two-photon process, we define a cutoff c such that all wave function populations of momenta k_1 and k_2 where $k_1^2 + k_2^2 < c^2$ are considered to be resulting from the single-photon process. Here c is chosen for an individual photon energy E as $c \gg \sqrt{2(E - I_p)}$, where I_p is the ionization potential for He. From this we find a single-photon double-ionization yield α from which we can calculate a corresponding cross section σ^{2+} as $\sigma^{2+} = \alpha\omega/\int_0^\infty I(t)dt$ [$I(t)$ is the intensity of the pulse at time t and ω is the frequency of the pulse].

The presence of excited bound states (both single-electron and double-electron) in the final-state wave function complicates the analysis of the final-state energy distributions of the two ejected electrons. As we are currently only interested in double-ionization wave packets, a Gaussian mask was applied to the wave function in the regions $r_1 < 35a_0$ and $r_2 < 35a_0$ to hide the singly bound states and in $r_1^2 + r_2^2 < (150a_0)^2$ for the doubly bound states. Care was taken to ensure that by the end of the time propagation, the final yield had stabilized with respect to time, indicating that all double-ionization wave packets had propagated into the unmasked area.

III. RESULTS

To demonstrate the capabilities of this method, five sets of photoionization data were calculated for pulses of photon energies 84, 99, 125, 150, and 180 eV and of peak intensity $4 \times 10^{14}\mathrm{W/cm^2}$. The pulse comprises 15 cycles (2 cycles of $\sin^2$ turn on, 11 cycles of constant peak intensity, and 2 cycles of $\sin^2$ turn off). A grid spacing of $\Delta x = 0.25a_0$ is used for both dimensions of the FD grid, and the boundary between the regions is placed at $b = 25a_0$. The propagator is a sixth-order Taylor series propagator with a time step of 0.028 as. A basis of 50 B splines is used to describe the single-electron functions in the inner region from which the two electron states were constructed. Two electron states with energies above 1000 a.u. were excluded from the calculations. Individual electrons are

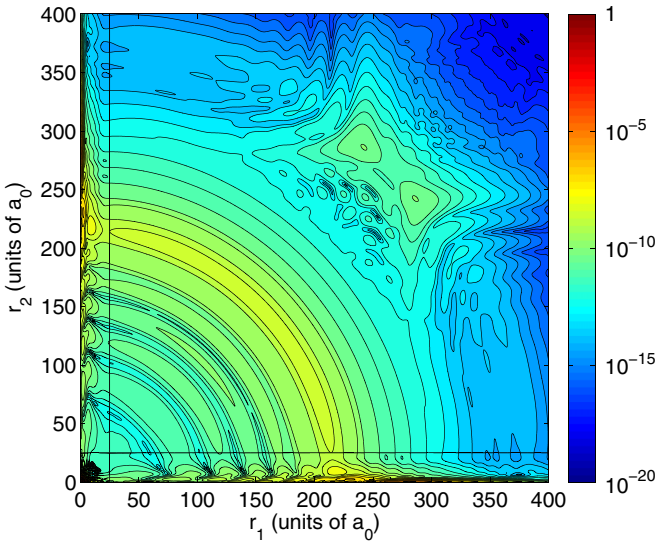

FIG. 1. (Color online) Two-electron helium wave function density (a_0^{-2}) 70 cycles after the end of a 15 cycle pulse. r_1 corresponds to the radial distance of electron 1 and r_2 corresponds to the radial distance of electron 2. The pulse has a photon energy of 150 eV and a peak intensity of 10^{14} W cm^{-2}. All distances are given in bohr radii (a_0). Boundaries at r_1,$r_2 = 25a_0$ divide the three RMT regions.

limited to a maximum angular momentum of $\ell = 3$ and the atom is limited to a maximum angular momentum of $L = 2$. The two-electron outer region is limited to $r_1 + r_2 \lesssim 900a_0$.

Figure 1 shows a two-electron wave function 70 cycles after the end of a 15-cycle laser pulse of photon energy 150 eV with the momentum transform for the large t limit calculated from this wave function given in Fig. 2. Data from Figs. 1 to 4

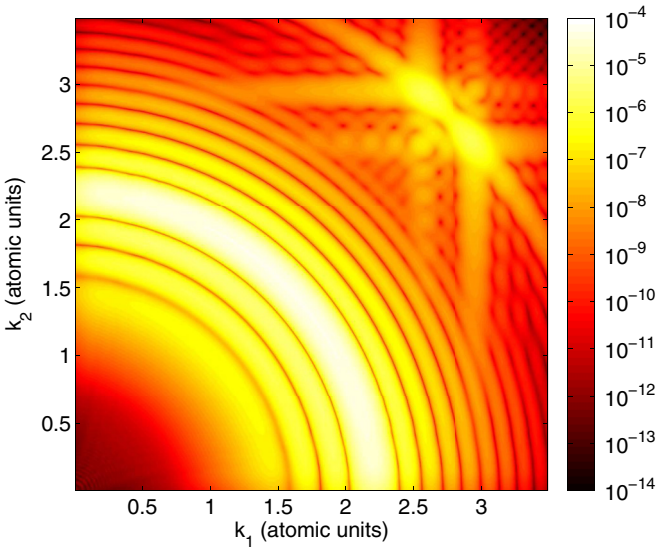

FIG. 2. (Color online) Two-electron probability distribution in momentum space calculated from the final-state wave function (shown in Fig. 1). k_1 corresponds to the radial momentum of electron 1 and k_2 corresponds to the radial momentum of electron 2. The pulse has a photon energy of 150 eV and a peak intensity of 10^{14} W cm^{-2}. All momenta are given in a.u.

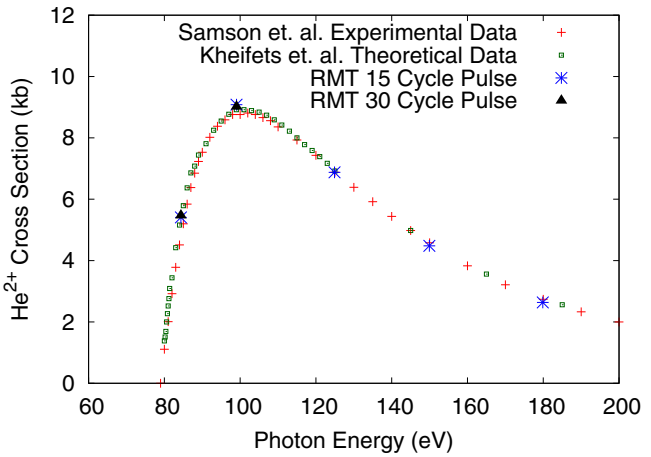

FIG. 3. (Color online) Single-photon double-ionization cross sections calculated using RMT alongside experimental data from Ref. [23] and theoretical data from Ref. [24].

can be accessed via Ref. [22]. A single-photon nonsequential process (where both electrons are simultaneously ionized by a single photon) is indicated in the momentum plot by the arc at $(k_1^2 + k_2^2) \approx (2.3 \text{ a.u.})^2$, as would be predicted given the necessary energy sharing for this process. This process is found in the corresponding wave function density (Fig. 1) in the arc in the region $r_1^2 + r_2^2 = (220a_0)^2$. In addition, evidence of a two-photon sequential process is seen in Fig. 1, with the outer and inner electrons at a distance of $\approx 300a_0$ and $\approx 250a_0$ from the nucleus, respectively. This process may also be seen in the momentum transform for k_1 and $k_2 \approx 3$ a.u.

Processes other than double ionization are also calculated using this approach, and their effects are visible in Fig. 1. Single ionization is visible close to axes r_1,$r_2 = 0$, and excitation to doubly excited states is visible near the nucleus, in addition to the remaining population in the ground state. While further information about these processes can in theory be extracted from the final wave-function data, none of these processes appear in the momentum transform due to the Gaussian mask acting on all non-double-ionization processes.

Figure 3 shows single-photon double-ionization cross sections obtained from a yield calculated using the momentum transform of the final wave functions. These data are given in comparison with experimental data [23] and theoretical data [24]. The theoretical RMT data follows the overall pattern of the experimental data, with the greatest disagreement ($\approx 15\%$) seen at 84 eV, reducing to $\approx 4\%$ at 125, 150, and 180 eV. To examine the effect of pulse length, cross sections were calculated at photon energies of 84 and 99 eV with a 30-cycle pulse (4 cycles ramp on and 4 cycles ramp off). Similar cross sections were calculated for both pulse lengths, indicating that the cause of the greater error at these photon energies lies elsewhere.

At low momenta, the double-ionized He^{2+} wave packet is difficult to distinguish from the long tails of higher-energy He^+ bound states. The calculation of the final double-ionization yield for these near-threshold photon energies most likely contains a contribution from these bound states. Since it is difficult to measure this contribution exactly without

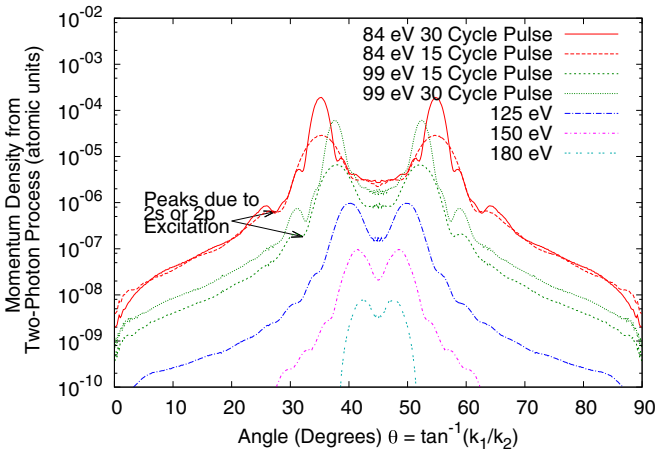

FIG. 4. (Color online) Two-photon momentum density across an arc corresponding to $c_{\min}^2 < k_1^2 + k_2^2 < c_{\max}^2$, where k_1 is the radial momentum of electron 1 and k_2 is the radial momentum of electron 2. Arrows indicating the expected angle of peaks caused by a sequential process involving an excitation of the un-ionized electron to $2s$ or $2p$ are shown for the 84- and 99-eV data.

propagating over a prohibitively large configuration space, we consider this effect to be a probable source of error. In addition, the differences between the current and the benchmark cross sections may be reduced by extending the range of angular momenta over which the wave function is represented.

To demonstrate that the RMT approach has the capacity to extract information about the two-photon sequential process (as well as the single-photon nonsequential process), a mask was applied to the momentum transform so that only the momentum density in the region $c_{\min}^2 < k_1^2 + k_2^2 < c_{\max}^2$ for the angular momentum couplings $L = 0$ and $L = 2$ was retained. $c_{\min}$ and $c_{\max}$ are given values according to the photon energy for the two-photon sequential double-ionization momenta (for example, for a photon energy of 150 eV in Fig. 2, $c_{\min} = 3.9$ a.u. and $c_{\max} = 4.2$ a.u.). The momentum density of the remaining arc is plotted against the angle $\theta = \tan^{-1}(k_1/k_2)$ in Fig. 4. These spectra are related to ejected-electron spectra, originally explored for sequential double ionization by Horner *et al.* [25], who showed their dependence on pulse length.

The two largest peaks in each photon energy are directly in the region expected for the sequential process where an electron is excited from the ground state into the continuum, leaving the bound electron in the He^+ $1s$ state which is ionized by a later photon. In the data for the 84- and 99-eV features an order of magnitude smaller are visible, which occur at momenta corresponding to a two-photon process (shown by the arrows in Fig. 4) where the bound He^+ electron is excited to either the $2s$ or $2p$ state before being ionized by the second photon (as discussed in detail in Refs. [26,27]). While these processes should also be present in the 125-, 150-, and 180-eV spectra, they occur at angles where the $1s$ process dominates, making them difficult to observe. The 30-cycle pulse data show these features more distinctly than the 15-cycle pulse data. For these longer pulses, an additional minimum is seen in the 84-eV spectra, corresponding to a sideband caused by the pulse length.

IV. CONCLUSIONS

In conclusion, we have combined a two-electron FD outer-region approach with the RMT method. This allows the double-ionized wave packet to be propagated over a larger configuration space. The accuracy of the approach is demonstrated by the determination of He single-photon double-ionization cross sections for photon energies in the region 80 to 180 eV. We obtain agreement with experiment and existing theory to within 15% near the single-photon double-ionization threshold and to within 4% for higher photon energies. The capability to investigate higher-order processes is demonstrated through the observation of signatures associated with a sequential ionization process involving excited states of the intermediate He^+ ion.

This agreement demonstrates the feasibility of attaching a two-electron FD region to an R-matrix outer region using the RMT methods and that this approach can be applied to predict a wide range of experimental observables. The FD method is highly parallelizable, and the current program scales linearly with the area covered by the two-electron double outer region.

The RMT method has the potential to study double ionization with full correlation in general atoms. For this potential to be realized, it will be necessary to develop a multielectron inner-region basis set with full correlation to model double ionization in the inner region, in addition to a corresponding outer-region basis set.

This research was sponsored by the Engineering and Physical Sciences Research Council (UK) under Grants No. EP/G055416/1 and No. EP/K029371/1 and by the Initial Training Network CORINF under a Marie Curie Action of the European Commission. This work used the ARCHER UK National Supercomputing service.

[1] P. B. Corkum and F. Krausz, Nat. Phys. **3**, 381 (2007).
[2] F. Krausz and M. Ivanov, Rev. Mod. Phys. **81**, 163 (2009).
[3] M. Yabashi, H. Tanaka, T. Tanaka, H. Tomizawa, T. Togashi, M. Nagasono, T. Ishikawa, J. Harries, Y. Hikosaka, A. Hishikawa *et al.*, J. Phys. B: At., Mol. Opt. Phys. **46**, 164001 (2013).
[4] B. Bergues, M. Kübel, N. G. Johnson, B. Fischer, N. Camus, K. J. Betsch, O. Herrwerth, A. Senftleben, A. M. Sayler, T. Rathje, T. Pfeifer, I. Ben-Itzhak, R. R. Jones, G. G. Paulus, F. Krausz, R. Moshammer, J. Ullrich, and M. F. Kling, Nat. Commun. **3**, 813 (2012).
[5] F. L. Yip, T. N. Rescigno, C. W. McCurdy, and F. Martín, Phys. Rev. Lett. **110**, 173001 (2013).
[6] K. Bartschat, E. T. Hudson, M. P. Scott, P. G. Burke, and V. M. Burke, J. Phys. B: At., Mol. and Opt. Phys. **29**, 115 (1996).
[7] P. G. Burke, C. J. Noble, and P. Scott, Proc. R. Soc. London, Ser. A **410**, 289 (1987).

[8] N. Scott, M. Scott, P. Burke, T. Stitt, V. Faro-Maza, C. Denis, and A. Maniopoulou, Comput. Phys. Commun. **180**, 2424 (2009).
[9] M. W. McIntyre, A. J. Kinnen, and M. P. Scott, Phys. Rev. A **88**, 053413 (2013).
[10] L. Moore, M. Lysaght, L. Nikolopoulos, J. Parker, H. Van Der Hart, and K. Taylor, J. Mod. Opt. **58**, 1132 (2011).
[11] M. A. Lysaght, L. R. Moore, L. A. A. Nikolopoulos, J. S. Parker, H. W. van der Hart, and K. T. Taylor, J. Phys.: Conf. Ser. **388**, 012027 (2012).
[12] L. A. A. Nikolopoulos, J. S. Parker, and K. T. Taylor, Phys. Rev. A **78**, 063420 (2008).
[13] H. F. Rey and H. W. van der Hart, Phys. Rev. A **90**, 033402 (2014).
[14] H. W. van der Hart and R. Morgan, Phys. Rev. A **90**, 013424 (2014).
[15] P. Burke, *R-Matrix Theory of Atomic Collisions: Application to Atomic, Molecular and Optical Processes*, Springer Series on Atomic, Optical, and Plasma Physics (Springer, New York, 2011).
[16] E. S. Smyth, J. S. Parker, and K. Taylor, Comput. Phys. Commun. **114**, 1 (1998).
[17] H. W. van der Hart, Phys. Rev. A **89**, 053407 (2014).
[18] M. Richter, M. Y. Amusia, S. V. Bobashev, T. Feigl, P. N. Juranić, M. Martins, A. A. Sorokin, and K. Tiedtke, Phys. Rev. Lett. **102**, 163002 (2009).
[19] A. S. Kheifets and I. Bray, J. Phys. B: At., Mol. Opt. Phys. **31**, L447 (1998).
[20] K. W. Meyer, C. H. Greene, and B. D. Esry, Phys. Rev. Lett. **78**, 4902 (1997).
[21] J. S. Parker, L. R. Moore, K. J. Meharg, D. Dundas, and K. T. Taylor, J. Phys. B: At., Mol. Opt. Phys. **34**, L69 (2001).
[22] http://pure.qub.ac.uk/portal/en/datasets/search.html.
[23] J. A. R. Samson, W. C. Stolte, Z.-X. He, J. N. Cutler, Y. Lu, and R. J. Bartlett, Phys. Rev. A **57**, 1906 (1998).
[24] A. S. Kheifets and I. Bray, Phys. Rev. A **54**, R995 (1996).
[25] S. Laulan and H. Bachau, Phys. Rev. A **68**, 013409 (2003).
[26] D. A. Horner, F. Morales, T. N. Rescigno, F. Martín, and C. W. McCurdy, Phys. Rev. A **76**, 030701 (2007).
[27] J. Feist, R. Pazourek, S. Nagele, E. Persson, B. I. Schneider, L. A. Collins, and J. Burgdrfer, J. Physics. B: At., Mol. Opt. Phys. **42**, 134014 (2009).